Reactions of HO_2 with *n*-propylbenzene and its phenylpropyl radicals

Mohammednoor Altarawneh*†, Bogdan Z. Dlugogorski

School of Engineering and Information Technology

Murdoch University, Perth, Australia

*Corresponding Author:

Phone: (+61) 8 9360-7507

E-mail: M.Altarawneh@Murdoch.edu.au

† On leave from Chemical Engineering Department, Al-Hussein Bin

Talal University, Ma'an, Jordan

Abstract

Abstraction of an H atom from the propyl side chain by hydroperoxyl radicals (HO_2) constitutes a central reaction in the low-temperature oxidation of *n*-propylbenzene (*n*PB). Herein, we calculate reaction rate constants for H abstraction from primary, secondary and benzylic sites in *n*PB. Rate of abstraction of a benzylic H atom dominates that of a secondary H atom with negligible abstraction of the primary H atom at $T \geq 600$ K. We present the reaction enthalpies for 1-phenyl-1-propyl (R1), 1-phenyl-2-propyl (R2) and 1-phenyl-3-propyl (R3) radicals, and compare the computed reaction rate constants and bond dissociation enthalpies with analogous scarce literature values. Addition of HO_2 radicals to radical sites in R1, R2 and R3 proceeds in a highly exothermic process and results in the formation of HO_2-phenylpropyl adducts. Mapped potential energy surfaces illustrate all plausible exit channels of the three HO_2-phenylpropyl adducts. Master equation calculations for the three phenylpropyl + HO_2 reactions indicate that direct O-OH bond fission and water elimination control the fate of the adducts leading to the formation of ketonic-type structures. Results from this study should be useful to update kinetic models for the low-temperature oxidation of alkylbenzenes in general.

Keywords: Hydroperoxyl radicals (HO_2); Alkyl aromatics; Quantum chemical modelling; Reaction rate constants.

1. Introduction

Alkyl aromatics represent a major fraction in various types of transportation fuels. Thus, congeners of alkyl aromatics may serve as surrogates replicating intrinsic chemical and physical properties of real fuels [1, 2]. In particular, *n*-propylbenzene (*n*PB) embodies well the properties of a class of alkyl benzenes in jet and diesel fuels [3, 4]. Previous studies have targeted several combustion characteristics of *n*PB, including ignition delay [5], laminar burning velocity [6] and sooting tendency [7]. The earlier work by Litzinger at al. [8] reported oxidation products at around 1060 K and 1 atm in a plug-flow reactor over various equivalence ratios. Dagaut et al. [9] produced profiles of stable species under atmospheric pressure and at temperatures between 900 and 1250 K. Roubaud et al. [5] performed rapid machine experiments on numerous alkylbenzenes, including *n*PB, over the low temperature range of 600 – 900 K. More recently, Brezinsky and Gudiyella investigated oxidative [10] and pyrolytic [11] decomposition of *n*PB at high pressure behind a reflected shock tube. Wang et al. [12] constructed temperature-dependent profiles of stable species, intermediates and radicals at low pressure. Chen and Froment [13] addressed thermal cracking of *n*PB at a temperature range of 893 – 1063 K and a pressure of 1.3 atm.

The aforementioned studies formulated detailed kinetic models of the combustion chemistry of *n*PB. As a consequence of scarcity of kinetic measurements pertinent to reactions of *n*PB with C_xH_y and O/H radicals, the studies adopted the reaction rate constants from analogous oxidation systems such as propane, ethylbenzene and toluene. In reference to thermal decomposition and pyrolysis of *n*PB, Robinson and Lindstedt reported theoretically-derived rate constants for abstraction of an H atom from the propyl side chain in *n*PB, by H and CH_3 radicals [14]. Darcy et al. [4] predicted the oxidation mechanism of *n*PB at low temperature

to be greatly influenced by the reaction sequence: RH + HO_2 → R + H_2O_2, H_2O_2 + M → 2OH + M. The authors have shown that at 1000 K, HO_2 and benzyl radicals govern the overall oxidation reactivity of *n*PB. This reaction sequence provides a corridor for the conversion of the relatively unreactive HO_2 radicals into the chain propagating radicals of OH [15, 16]. Whilst the reaction RH + HO_2 → R + H_2O_2 exhibits a central role in low-temperature oxidation mechanisms of alkyl benzenes, the addition of HO_2 to phenylalkyl radicals holds comparable prominence. The work of Metcalfe et al. [17] on oxidation of toluene and Darcy et al. on oxidation of *n*PB [18] demonstrated that, addition of HO_2 to benzyl radical represents the most important reactivity-promoting reaction. Kinetic data for this reaction were extracted from oxidation models on alkanes.

To the best of our knowledge, no kinetic measurements exist for H abstraction from the propyl side chain in the *n*PB molecule or for subsequent addition of HO_2 to the three possible phenylpropyl radicals. The two-part study of Scott and Walker [19, 20] appears to provide the sole estimate of the rate constants for two alkyl benzenes; i.e., toluene (benzyl) and ethylbenzene (1-phenylethyl). Thus, the aim of this study is twofold: firstly, to derive reaction rate constants for H abstraction from the three distinct C-H propyl sites in *n*PB by HO_2 radicals; and, secondly, to investigate the unimolecular decomposition of HO_2-phenylpropyl adducts. This work complements our ongoing interest in deriving reaction rate constants for H abstraction by HO_2 radicals [21, 22].

2. Computational details

Gaussian09 suite of programmes [23] expedited all structural optimisations and energy calculations at the composite theoretical method of CBS-QB3 [24]. The CBS-QB3 method facilitated the initial geometry optimisations and frequency calculations at the B3LYP/CBSB7 level, followed by several successive computations of single-point energies, at very accurate theoretical levels. Aguilera-Iparraguirre et al. [25] found that energy barriers for H abstractions by HO_2 radicals from C_1-C_4 alkanes vary significantly with the adopted theoretical approach. Their reaction rate constants, estimated based on computed activation energies at the CCSD(T)/cc-pVTZ level, were in accord with corresponding data calculated by Carstensen et al. [26] using the CBS-QB3 composite method.

We also calculated the standard enthalpies of formation by the G3MP2B3 composite method [27], and derived the rate constants by applying the conventional transition state theory. The one-dimensional Eckart formula served to correct the transmission coefficients for the quantum tunnelling effect [28]. For *n*PB + HO_2 reactions, we also estimated the transmission coefficients based on the Wigner equation [29]. Reaction pathways of selected transition structures were confirmed by the calculations of the intrinsic reaction coordinates (IRC).

The KiSThelp code aided the computation of the rate constants [30] at the high-pressure limit, with the internal rotations in reactants and transition structures treated as hindered rotors. Overall barriers of internal rotations (mainly -CH_3, -CH_2CH_3, -$CH_2CH_2CH_3$ and -OH) were obtained by performing partial optimisations and dihedral energy scans in reactants and transition structures, correspondingly. Energy calculations and derivation of reactions rate constants for alkanes and other alkylbenzenes systems involved the same theoretical

approaches (i.e. CBS-QB3 for structural optimisations and the KiSThelp code for estimations of reaction rate constants).

We completed master equation (ME) calculations for the three phenylpropyl + HO_2 systems using the MESMER code [31]. MESMER solves energy-grained ME to yield time-dependent concentrations and phenomenological (i.e. pressure-dependent) rate coefficients based on a procedure described by Bartis and Widom [32]. MESMER implements the conventional RRKM theory [33] for reactions with well-defined transition structures and the inverse Laplace transform (ILT) formalism for barrierless reaction [34]. For helium as a buffer gas, the exponential-down model deploys a $\langle \Delta E \rangle_{\text{down}}$ value of 500.0 cm^{-1}. Lennard-Jones parameters for all reactants were adapted from analogous values of toluene [35].

3. Results and discussion

3.1. Geometries and enthalpies of formation for nPB and its three derived phenylpropyl radicals

Aromatic C-H bonds in alkyl benzenes are significantly stronger (~ 110.0 kcal mol^{-1}) than those in the alkyl side chain [36]. Scissions of benzylic, secondary and primary C-H bonds in *n*PB afford 1-phenyl-1-propyl (R1), 1-phenyl-2-propyl (R2) and 1-phenyl-3-propyl (R3) radicals, respectively. Species identification by synchrotron vacuum ultraviolet photoionisation mass spectrometry (VUV-MS) confirmed the formation of R1, R2 and R3 radicals in a rich premixed flame of *n*PB at low pressure [37]. Figure 1 depicts geometries of the *n*PB molecule and the three phenylpropyl radicals.

Available estimates of all bond dissociation enthalpies (BDH) and standard enthalpies of formation ($\Delta_f H°_{298}$) of the three phenylpropyl radicals originate from a thermochemical compilation of Dagaut et al. [9]. Isodesmic reactions of IR1-IR4, illustrated in Scheme 1, provide updated values of BDH and $\Delta_f H°_{298}$ for R1-R3 radicals and represent a benchmark for the accuracy of our reported thermochemical values:

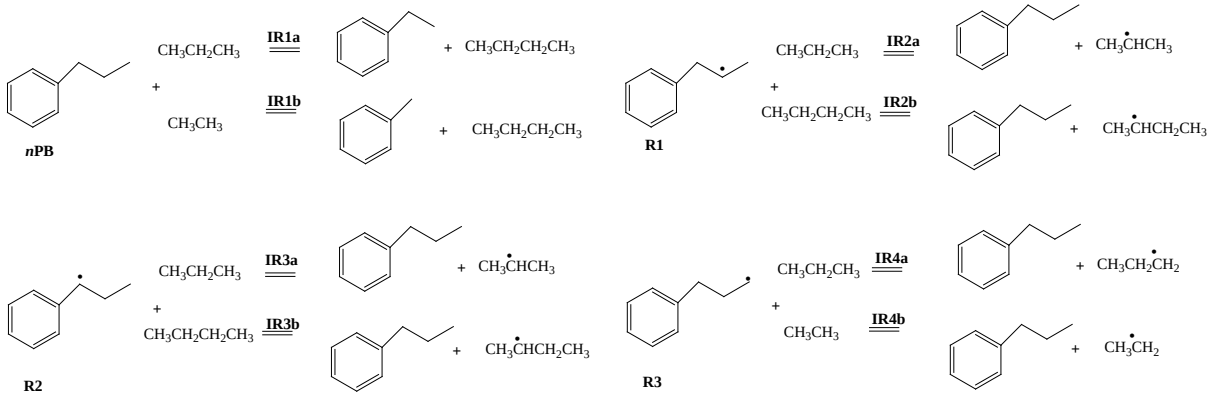

Scheme 1

Table 1 lists $\Delta_f H°_{298}$ for reference species incorporated in the isodesmic reactions of IR1-IR4. We have adopted the approach of Simmie et al.[38] to report the calculated $\Delta_f H°_{298}$ values ($\bar{x}$) and their associated uncertainty limits (u_j). In this procedure, the uncertainty u_j in $\Delta_f H^o_{298}$, for each of the target species in the isodesmic reaction *j*, is calculated as $u_j=(\Sigma u_i^2)^{1/2}$, where u_i refers to the uncertainty in the experimental values of $\Delta_f H^o_{298}$ of reference species appearing in the isodesmic reaction *j*. Final enthalpies, ($\bar{x}$), are written as weighted grand mean of $\sum(x_j/u_j^2)/\sum(1/u_j^2)$ where x_j denote the mean of the $\Delta_f H^o_{298}$ values, obtained from the two isodesmic reactions. Lastly, the overall uncertainty, ($\bar{u}$), is expressed as $1/[\sum(1/u_j^2)]^{1/2}$

.

Values of $\Delta_f H°_{298}$ for R1, R2 and R3 radicals equal 39.6 ± 1.2 kcal mol^{-1}, 48.6 ± 0.4 kcal mol^{-1} and 51.0 ± 0.5 kcal mol^{-1}, in that order. As Table 2 shows, estimated $\Delta_f H°_{298}$ for R2 and R3 are in good agreement with corresponding limited appraisals in literature [9]. However, the calculated $\Delta_f H°_{298}$ for R1 slightly overshoots the estimate of Dagaut et al. by ~ 4.0 kcal mol^{-1} [9]. The computed standard enthalpies of formation at 298.15 K for *n*PB, as well as for R1, R2 and R3 radicals yield BDHs of 89.1 kcal mol^{-1}, 98.2 kcal mol^{-1} and 100.6 kcal mol^{-1}, for benzylic, secondary, and primary C-H bonds, respectively. The latter two accord with those reported by Dagaut et al. of 100.0 kcal mol^{-1} and 99.0 kcal mol^{-1} [9]. The estimated BDH for benzylic C-H bond matches very well that of toluene, i.e. 90.0 kcal mol^{-1} [36]. The resonance stabilised primary radical of R1 displays a noticeable difference in BDH in comparison to the genuine secondary and primary radicals of R2 and R3, respectively.

3.2. Abstraction of propyl H atom by HO_2 radicals

Our recent work on reactions between HO_2 radicals and ethyl benzene [22] has demonstrated that, addition of HO_2 to the phenyl ring or abstraction of an aromatic H atom is of negligible significance, if compared with the dominant channels entailing H abstraction from the ethyl chain. We limit our analysis of the *n*PB + HO_2 system to the most important propyl H abstraction channels. Activation enthalpies for H abstraction of benzylic, secondary and primary sites amount to 13.0 kcal mol^{-1}, 13.2 kcal mol^{-1} and 17.5 kcal mol^{-1}, respectively, and the corresponding reaction enthalpies to 1.4 kcal mol^{-1}, 11.8 kcal mol^{-1} and 14.5 kcal mol^{-1}. Despite of the remarkable difference in BDH between secondary and benzylic C-H bonds (99.0 versus 90.0 kcal mol^{-1}), abstraction of H atoms from both sites incurs very similar

activation enthalpies. Table 3 presents the fitted Arrhenius parameters for all three H abstraction channels, whereas Fig. 2 portrays their branching ratios. At temperatures lower than 600 K, abstraction from a secondary position holds more importance than abstraction from benzylic site, but, at higher temperatures, the latter becomes the dominant pathway. The relative contribution of the primary C-H channel gradually increases to reach 0.10 at 1000 K. Reaction rate parameters in Table 3 and branching ratios in Fig. 2 indicate that, H abstraction from the propyl side chain, by HO_2, produces R1 and R2 radicals in competing pathways with small, but not negligible, product flux into R3 at temperatures relevant to low-temperature oxidation of *n*PB, i.e. $T \leq 1000$ K.

To the best of our knowledge, literature provides no theoretical or experimental estimations of rate constants for the *n*-propylbenzene + HO_2 reaction. Thus, we elect to compare our calculated values for the system at hand with corresponding literature values for systems of propane, toluene and ethyl benzene. Figure 3 compares our calculated reaction rate constants of the three channels with the corresponding values deployed in kinetic models of Dagaut et al. [9] and Gudiyella and Brezinsky [11]. These two models incorporate the kinetic parameters that were carried over from the system of *n*-propane + HO_2 based on the recommended values of Baulch et al. [39], from primary and secondary sites and from the system of toluene + HO_2 for benzylic sites [39]. Comparison is also made with our theoretically-derived values for ethylbenzene [22]. Whilst our calculated estimates at low temperature substantially deviate from the other three sets of data, all appraisals coincide for $T \geq 600$ K. For example, as depicted in Fig. 3c, evaluated reaction rate constants for H abstraction from a benzylic site fall within a multiplication factor of 0.14-2.54 of rate constants available in literature, over the entire low-temperature oxidation window of 600 K – 1200 K. Our kinetic parameters for H abstraction from primary and secondary sites in *n*PB

remain in a reasonable agreement with the corresponding data for propane compiled by Tsang [40]. For instance at 600 K and 800 K, we estimate reaction rate constants for H abstraction from primary sites in *n*PB to be 9.85×10^{-19} cm^3 $molecule^{-1}$ s^{-1} and 2.76×10^{-17} cm^3 $molecule^{-1}$ s^{-1}, correspondingly, whereas analogous values for propane [40] are 3.12×10^{-19} cm^3 $molecule^{-1}$ s^{-1} and 2.08×10^{-17} cm^3 $molecule^{-1}$ s^{-1}, in that order.

In our recent study on ethylbenzene + HO_2 system [22], we have shown that, abstraction of a primary H atom incurs very similar activation energies if compared with alkanes. In order to elucidate the dependency of kinetics parameters pertinent to H abstraction by HO_2, on the length of alkyl chain and/or the presence of an aromatic chain, we calculate reaction rate constants for H abstraction from primary and secondary carbons in C_3-C_5 alkanes and compare these results with analogous values for C_1-C_3 alkyl benzenes. Table 4 reports the calculated reaction and activation enthalpies, fitted Arrhenius parameters and reaction rate constants at selected temperatures for H abstractions from primary and secondary positions in C_3-C_5 alkanes and C_2-C_3 alkyl benzenes and from benzylic positions in C_1-C_3 alkyl benzenes per C-H site. As evident from the calculated values in Table 4, the length of the alkyl chain in both alkanes and alkyl benzenes exhibit minimal influence on the calculated reaction rates. Moreover, the presence of the phenyl ring exerts only a slight difference, seen by comparing the estimated kinetic parameters for alkyl benzenes with the analogous values of alkanes.

While estimated activation energy for H abstraction from benzylic positions in toluene (12.2 kcal mol^{-1}) matches corresponding values for ethylbenzene (12.3 kcal mol^{-1}) and *n*-propylbenzene (12.1 kcal/mol), *A*-factor for H abstraction from benzylic positions in ethylbenzene and *n*-propylbenzene exceeds that of toluene by factors of 4.6 and 12.6,

respectively. In order to elucidate a plausible explanation, Figure S1 in the supplementary material plots the entropy of activation ($\Delta S^{\#}$) for the abstraction of benzylic H atoms from toluene and *n*-propylbenzene over the temperature interval of 300 - 800 K. $\Delta S^{\#}$ values for the reaction of toluene + HO_2 → benzyl + H_2O_2 are considerably lower (i.e. more negative) than analogous values for the reaction of *n*-propylbenzene + HO_2 → R1 + H_2O_2.

At 773 K, Scott and Walker [20] found that the reaction of toluene + HO_2 → benzyl + H_2O_2 proceeds at a rate of $8.82 \pm 2.40 \times 10^{-17}$ cm^3 $molecule^{-1}$ s^{-1}, whereas the overall rate for the reaction ethylbenzene + HO_2 → 1-phenylethyl/2-phenylethyl + H_2O_2 corresponds to $2.64 \pm 1.04 \times 10^{-16}$ cm^3 $molecule^{-1}$ s^{-1}. At the same temperature, our calculated rate constant for the overall reactions of toluene + HO_2 and ethylbenzene + HO_2 are estimated to be 2.42×10^{-17} cm^3 $molecule^{-1}$ s^{-1} and 9.71×10^{-17} cm^3 $molecule^{-1}$ s^{-1}. Considering the reported uncertainty limits in the two experimental measurements for toluene (i.e. $\pm 2.40 \times 10^{-17}$ cm^3 $molecule^{-1}$ s^{-1}) and ethylbenzene ($\pm 1.04 \times 10^{-16}$ cm^3), our calculated rate constants for the two systems are in satisfactory agreements with the analogous experimental measurements. Scott and Walker [20] found that the rate constant for the reaction of HO_2 with ethylbenzene exceeds that of toluene by a factor of 3.0, while our corresponding prediction amounts to a factor of 4.3. A faster overall rate constant for the reaction ethylbenzene + HO_2, in reference to that of toluene + HO_2, stems not only from a larger number of abstractable H sites in ethyl benzene but also from a lower *A* factor in the toluene system.

Aguilera-Iparraguirre et al. [25] calculated theoretically reaction rate constants for H abstractions by HO_2 radicals from the two distinct positions in propane, and *n*-butane, and contrasted their estimations with analogous theoretically derived values of Carstensen et al. [26] and recommended values of Orme et al. [41], Baldwin et al. [42], and Scott and Walker

[20]. Aguilera-Iparraguirre et al. [25] found that their calculated values reasonably agree with these four sets of data. To benchmark the accuracy of our rate constants calculated for *n*-propylbenzene + HO_2 reaction, Table 4 also compares our results with those of Aguilera-Iparraguirre et al. [25] for propane and *n*-butane. As evident from Table 4, our values coincide with the corresponding data of Aguilera-Iparraguirre et al. [25] within the multiplication factors of ~ 1.00 - 2.80.

3.3. Unimolecular decomposition of the three hydroperoxyl-phenylpropyl adducts

While alkyl benzene radicals readily isomerise at elevated temperatures or undergo C-H/C-C bond scissions, they are relatively long-lived species at low to intermediate temperatures. This enables alkyl benzene radicals to interact with reactive species in the combustion media. Additions of molecular oxygen to benzylic sites in phenylalkyl proceed in barrierless processes [43], i.e. backward reactions into phenylalkyl + O_2 dominate unimolecular isomerisations of phenylalkyl peroxy radicals. As a result, addition of HO_2 to the three radical sites in R1, R2 and R3 constitutes an active oxidation corridor, especially at low temperatures prior to the establishment of the reactive radical pool. Herein, we investigate unimolecular transformations of the three HO_2-phenylpropyl adducts.

3.3.1 Potential energy surfaces (PESs)

Addition of HO_2 to radical sites in R1, R2 and R3 proceed with excess energies of 60.8 kcal mol^{-1}, 73.1 kcal mol^{-1} and 72.1 kcal mol^{-1}, respectively. Products from these combination reactions are the three HO_2-phenylpropyl adducts of M1, M2 and M3, correspondingly.

Figures 4-6 depict all plausible exit channels for the highly energised M1, M2 and M3, featuring reverse reactions back into separated reactants, direct fissions of O-OH bonds, and unimolecular elimination of OH and H_2O.

Figure 4 illustrates the six unique exit pathways for the M1 adducts. Barrierless direct ruptures of C-OOH and O-OH bonds require endothermicity of 60.8 kcal mol^{-1} and 43.1 kcal mol^{-1}, in that order. These two BDH values match very well the corresponding value calculated for the benzyl-OOH system, i.e. 60.0 kcal mol^{-1} and 43.0 kcal mol^{-1}, correspondingly [44]. Fission of the O-OH bond produces the benzoxyl-type intermediate of M5 and an OH radical. The latter could also arise via the transition structure TS3, in a process that comprises a 1,2-hydrogen shift from the benzylic carbon atom to the inner oxygen atom simultaneously with elimination of the hydroxyl group from the OOH moiety. The enthalpic barrier of TS3 amounts to 48.2 kcal mol^{-1}. Products from this channel (M6 and OH) reside 16.3 kcal above M1. An OH shift from the hydroperoxy moiety to an *ortho* ring position affords the M7 intermediate through an elevated enthalpic barrier of 59.5 kcal mol^{-1} (TS4). TS5 marks elimination of a water molecule in which the terminal OH group abstracts an *ortho* H atom from the aromatic ting. TS5 is associated with a considerable enthalpic barrier of 73.1 kcal mol^{-1}. In view of the prohibitive reaction energetics required by TS4 and TS5, we do not explore further the decompositions of the M7 and M8 moieties. Elimination of a water molecule from M1 produces a propiophenone molecule (M4) through two distinct transition structures, TS1 and TS2.

Figure 7 exhibits atomic movements in TS1 and TS2. In the three-centred structure of TS1, the terminal OH group departs the M1 intermediate along with a hydrogen atom from the benzyl site. In TS2, a water molecule is expelled via elimination of the outer OH group and a

hydrogen atom from a secondary carbon atom accompanied by a 1,2-hydrogen shift from the benzylic carbon to the secondary carbon. The enthalpic barrier associated with TS1 corresponds to 42.4 kcal mol^{-1}, i.e. slightly lower, by 4.6 kcal mol^{-1}, in reference to the barrier of TS2. The formed propiophenone and water molecules lie in a significant potential well of 64.4 kcal with respect to the entrance channel. Finally, C-C bond fission in M5 affords benzaldehyde (M9) and an ethyl radical. This step encounters a smaller energy barrier than C-C bond fission yielding phenyl radical and propionaldehyde, viz. 5.1 kcal mol^{-1} (TS6) versus 18.7 kcal mol^{-1} (TS7).

Decomposition of the HO_2-phenylpropyl M2 and M3 adducts exhibits very similar mechanistic and energetics features to that of M1. Fission of O-OH bonds in M2 and M3 appears to be equally endothermic at 43.7 kcal mol^{-1} and 42.9 kcal mol^{-1} and results in the formation of M11 and M17 moieties, correspondingly. Concerted elimination of OH from M2 and M3 occurs through TS10 and TS15 and demands 45.5 kcal mol^{-1} and 52.3 kcal mol^{-1} as activation enthalpies, respectively. Preferred pathways for direct eliminations of water from M2 and M3 require very similar activation enthalpies, i.e. 38.4 kcal mol^{-1} (TS8) and 38.6 kcal mol^{-1} (TS13), respectively. The intermediates of M11 and M17 could readily dissociate into benzyl and 2-ethylphenyl radicals.

3.3.2. Reaction kinetics

3.3.2.1. High-pressure limit reaction rate constants

Table 5 assembles the calculated kinetic parameters at the high-pressure limit for all elementary reactions governing the unimolecular decompositions of M1 (Fig. 4), M2 (Fig. 5)

and M3 (Fig. 6). We fit the reaction rate constants in the temperature range of 300 – 1500 K at the high-pressure limit. Estimating reaction rate constants for barrierless fission of the C-OOH and O-OH bonds necessitates treatment by the variational transition state theory (VTST) [45]. However, CBS-QB3 composite method could not establish the reliable minimum energy point (MEP) curve along the assigned stretching of the C-OOH/O-OH bonds. This is primarily due to the fact that, functionals composing the CBS-QB3 method comprise single-reference determinants that cannot handle satisfactorily singlet-triplet crossings involved in radical-radical bond fissions.

In previous studies, we utilised a Morse curve [46] and the Yamagushi approximated spin-projection scheme [47] to construct MEP curves. In both cases, we found fitted activation energy from calculations of VTST to be very close to the corresponding reaction energy (i.e. within 1.0 – 3.0 kcal mol^{-1}). Thus, herein we assume that, transition structures for the C-OOH and O-OH bond fissions occur when their energies on triplet surfaces are essentially the same as the corresponding reaction energies. The locations of these candidate structures of the transition-states occur at separation of between 2.60 Å - 2.90 Å and 3.00 Å – 3.20 Å, for fissions of the C-OOH and O-OOH bonds, respectively. These values concur with the corresponding distances determined by da Silva and Bozzelli in the system of benzyl + HO_2 [44]. Because of this treatment, larger *A* factors (i.e. longer separations) in the Arrhenius formula compensate any errors arising from setting the activation energies to match exactly the reaction energies. The structures of these transition states still hold one and only one imaginary frequency along the specified reaction coordinate.

Existing kinetic models for oxidation of *n*PB assumed that, reactions between HO_2 and phenylpropyl radicals proceed by two pathways [9, 11]:

$C_6H_5CHCH_2CH_3 + HO_2 \rightarrow OH + C_2H_5 + C_6H_5C(H)O$ Rx1

$C_6H_5CH_2CHCH_3 + HO_2 \rightarrow OH + CH_3C(H)O + C_6H_5CH_2$ Rx2

Rx1 has an overall reaction rate expression of $k(T) = 8.30 \times 10^{-13} \exp(-2\,000/T)$ cm^3 molecule^{-1} s^{-1}, whereas a temperature-independent rate constant of 8.30×10^{-13} cm^3 molecule^{-1} s^{-1} describes the rate of Rx2. Both rate constants originate from *n*-propyl + HO_2 system. PESs, depicted in Figs. 4 and 5, confirm the occurrence of these two sequences as the most preferred pathways for reactions of HO_2 with R1 and R2 radicals. Overall barriers for Rx1 and Rx2 lie 12.6 kcal mol^{-1} (i.e. height of TS6 with respect to R1 + HO_2 in Fig. 4) and 24.4 kcal mol^{-1} (i.e. height of TS12 with respect to R2 + HO_2 in Fig. 5) *below* their corresponding separated reactants. This finding agrees with the very low energy of activation (i.e. 4 kcal mol^{-1} for Rx1) and the temperature-independent reaction rate constant (for Rx2) deployed in available kinetic models for reaction of HO_2 with phenylpropyl radicals. The fast reaction rate constants calculated for β C-C bond fissions in M5, M11 and M17 indicate that, these intermediates are unlikely to participate in the bimolecular H-abstraction reaction RO˙ + R`H → ROH + R`, because of their short lifetimes.

Table 6 lists reaction rate parameters for the bimolecular addition of HO_2 to radical sites in R1, R2 and R3. Our calculations have yielded the negative activation energies for the three bimolecular reactions. Predicted negative values of activation energies arise from the profound exothermic reaction enthalpies for these three reactions. A negative activation energy has also been reported for the reaction HO_2 + benzyl [44]. A lower *A* factor reflects the HO_2 addition to the electron-delocalised radical R1. The experimental study by Ellis et al. [19] reported the HO_2 addition to benzyl radical to occur via a temperature-independent

reaction rate constant of 8.30 ± 3.35 × 10^{-13} cm^3 $molecule^{-1}$ s^{-1}. Our calculated reaction constant for the HO_2 + R1 association reaction at 800 K deviates from experimental measurement for HO_2 + benzyl, by almost an order of magnitude. Accurate determination of reaction rate constant involving HO_2 addition to radicals requires simultaneous measurements of time-histories of H/O species in addition to that of the target radical [48]. However, Ellis et al. [19] did not measure their rate constant directly (i.e. shock tube/laser absorption techniques) but rather via detailed fitting to a complex reaction mechanism describing trace amounts of toluene in a mixture of H_2 + O_2. The significant uncertainty limit in the reaction rate constant (i.e. ± 3.35 × 10^{-13} cm^3 $molecule^{-1}$ s^{-1}) reflected a plausible interference by the reactive O/OH species [19]. Furthermore, it is a challenging task to determine experimentally a rate constant for a radical-radical combination reaction, especially in case of a significant population of transient HO_2 radicals [49].

3.3.2.2. Time-dependent concentrations and phenomenological rate coefficients

Table 7 enlists phenomenological rate coefficients at 1.0 atm and three selected temperatures for the most significant reactions in the three phenylpropyl + HO_2 systems. Figures 8, 9 and 10 depict time-dependent species profiles for systems of R1 + HO_2, R2 + HO_2 and R_3 + HO_2, respectively at 1.0 atm as calculated by the MESMER code. It is envisaged from the product profiles in Figs. 8-10 that, the O-OH direct bond fission constitutes most significant channel operating in the unimolecular decomposition of M1, M2 and M3 adducts at all operational conditions. da Silva and Bozzelli [44] also predicted the O-OH bond scission to dominate the unimolecular decomposition of the benzylhydroperoxide adduct. Profiles of product species illustrated in Figure 8 confirm that water elimination and formation of the M4

molecule contribute significantly to the R1 + HO_2 reaction at all temperatures. The analogous channel in the R3 + HO_2 reaction becomes important only at low temperatures. Constructed product profiles herein match the corresponding branching ratios based on the high-pressure limit reaction rate constants given in Table 5.

Having discussed product profiles from the three phenylpropyl + HO_2 systems, we are now in a position to elaborate on their plausible importance in oxidation of *n*PB:

- Our plotted time-dependent product profiles reveal that phenylpropyl + HO_2 reactions result predominantly in the formation of the OH flame-propagating radicals. It follows that these addition reactions serve as a potential source for OH radicals, beside the commonly prevailing low-temperature mechanism of (HO_2 + HO_2 → H_2O_2 + O_2, H_2O_2 + M → 2OH).

- Reactions leading to the formation of the three phenylpropyl ketonic-structures (M4, M10, M15) contribute meaningfully to the fate of the three HO_2-phenylpropyl adducts, yet they are not included in available kinetic models [43].

- As addition of oxygen molecule to benzylic site in alkyl benzenes is highly reversible, the exothermic reaction sequence HO_2 + R1 → M1 → M5 + OH → M9 + OH + C_2H_5 constitutes an important source of the formation of benzaldehyde (M9) that is detected experimentally from oxidation of *n*PB [11].

- The kinetic model of Darcy et al. [18] found the reactions involving HO_2 to display a strong promoting effect on oxidation; especially, the reaction of benzyl + HO_2 →

$C_6H_5CH_2O$ + OH. As Figure 6 demonstrates, the most accessible channel for R3 + HO_2 produces the benzyl radical.

- In an analogy to the benzyl radical, the resonance-stabilised radical of R1 is expected to be a long-lived species enabling its reaction with HO_2 in the low/intermediate temperature interval.

4. Conclusions

Similar activation enthalpies and reaction rate constants are obtained for H abstraction by HO_2 radicals from primary and secondary carbons in alkanes and alkyl benzenes. Bond dissociation enthalpies for benzylic, secondary and primary C-H in *n*PB amount to 89.1 kcal mol^{-1}, 98.2 kcal mol^{-1} and 100.6 kcal mol^{-1}, correspondingly. Despite a noticeable difference in the bond dissociation energies between benzylic and secondary H atoms in the *n*-propylbenzene molecule, H abstraction from these two positions by HO_2 radicals incur rather comparable reaction rate constants. Abstraction of a benzylic H atom from a toluene molecule proceeds at a slower reaction rate constants if compared with ethyl benzene and *n*-propylbenzene. We discuss this discrepancy in view of the limited experimental measurements available for HO_2 reaction with toluene and ethyl benzene. The presence of the aromatic ring exerts a minimal effect on kinetic parameters for abstraction of a secondary or primary H atom from alkylbenzenes in reference to corresponding sites in alkanes. HO_2-phenylpropyl adducts branch into several channels comprising mainly eliminations of OH and H_2O. We constructed time-dependent products profiles at 1.0 atm by solving the master equation for the three predict the three-phenylpropyl + HO_2 reaction systems. These calculations predict the direct O-OH bond fissions to dominate the exit channels available for

the three HO_2-phenylpropyl adducts under all considered temperature and pressure conditions, albeit, with further significant product flux into ketonic phenylpropyl structures, especially in the reaction R1 + HO_2.

Supplementary information available

Figure S1. CBS-QB3 thermal enthalpies, Cartesian coordinates, vibrational frequencies and rotational constants and NASA polynomials of structures presented in the manuscript.

Acknowledgments

The Australian Research Council (ARC), the National Computational Infrastructure (NCI), Australia, and the iVEC supercomputing facilities in Perth have supported this study.

References

[1] S. Dooley, S.H. Won, M. Chaos, J. Heyne, Y. Ju, F.L. Dryer, K. Kumar, C.-J. Sung, H. Wang, M.A. Oehlschlaeger, R.J. Santoro, T.A. Litzinger, Combust. Flame 157 (2010) 2333-2339.
[2] H. Nakamura, D. Darcy, M. Mehl, C.J. Tobin, W.K. Metcalfe, W.J. Pitz, C.K. Westbrook, H.J. Curran, Combust. Flame 161 (2014) 49-64.
[3] D. Darcy, H. Nakamura, C.J. Tobin, M. Mehl, W.K. Metcalfe, W.J. Pitz, C.K. Westbrook, H.J. Curran, Combust. Flame 161 (2014) 65-74.
[4] D. Darcy, H. Nakamura, C.J. Tobin, M. Mehl, W.K. Metcalfe, W.J. Pitz, C.K. Westbrook, H.J. Curran, Combust. Flame 161 (2014) 1460-1473.
[5] A. Roubaud, R. Minetti, L.R. Sochet, Combust. Flame 121 (2000) 535-541.
[6] C. Ji, E. Dames, H. Wang, F.N. Egolfopoulos, Combust. Flame 159 (2012) 1070-1081.
[7] C.S. McEnally, L.D. Pfefferle, Combust. Flame 148 (2007) 210-222.
[8] T.A. Litzinger, K. Brezinsky, I. Glassman, Combus. Sci. Technol. 50 (1986) 117-133.
[9] P. Dagaut, A. Ristori, A. El Bakali, M. Cathonnet, Fuel 81 (2002) 173-184.
[10] S. Gudiyella,K. Brezinsky, Proc. Combust. Inst. 34 (2013) 1767-1774.
[11] S. Gudiyella, K. Brezinsky, Combust. Flame 159 (2012) 940-958.

[12] Z. Wang, Y. Li, F. Zhang, L. Zhang, W. Yuan, Y. Wang, F. Qi, Proc. Combust. Inst. 34 (2013) 1785-1793.
[13] Q. Chen,G.F. Froment, J. Anal. Appl. Pyrol. 21 (1991) 51-77.
[14] R.K. Robinson,R.P. Lindstedt, Combust. Flame 160 (2013) 2642-2653.
[15] J. Zádor, C.A. Taatjes, R.X. Fernandes, Prog. Energy. Combust. Sci. 37 (2011) 371-421.
[16] R.W. Walker,C. Morely, Low-Temperature Combustion and Autoignition 1997: Elsevier.
[17] W.K. Metcalfe, S. Dooley, F.L. Dryer, Energy Fuel 25 (2011) 4915-4936.
[18] D. Darcy, C.J. Tobin, K. Yasunaga, J.M. Simmie, J. Würmel, W.K. Metcalfe, T. Niass, S.S. Ahmed, C.K. Westbrook, H.J. Curran, Combust. Flame 159 (2012) 2219-2232.
[19] C. Ellis, M.S. Scott, R.W. Walker, Combust. Flame 132 (2003) 291-304.
[20] M. Scott,R.W. Walker, Combust. Flame 129 (2002) 365-377.
[21] M. Altarawneh, B.Z. Dlugogorski, E.M. Kennedy, J.C. Mackie, Combust. Flame 157 (2010) 1325-1330.
[22] M.K. Altarawneh, B.Z. Dlugogorski, E.M. Kennedy, J.C. Mackie, Combust. Flame 160 (2013) 9-16.
[23] Gaussian 09, M.J.T. Frisch, G. W.; Schlegel, H. B.; Scuseria, G. E.; Robb, M. A.; Cheeseman, J. R.; Scalmani, G.; Barone, V.; Mennucci, B.; Petersson, G. A.; Nakatsuji, H.; Caricato, M.; Li, X.; Hratchian, H. P.; Izmaylov, A. F.; Bloino, J.; Zheng, G.; Sonnenberg, J. L.; Hada, M.; Ehara, M.; Toyota, K.; Fukuda, R.; Hasegawa, J.; Ishida, M.; Nakajima, T.; Honda, Y.; Kitao, O.; Nakai, H.; Vreven, T.; Montgomery, Jr., J. A.; Peralta, J. E.; Ogliaro, F.; Bearpark, M.; Heyd, J. J.; Brothers, E.; Kudin, K. N.; Staroverov, V. N.; Kobayashi, R.; Normand, J.; Raghavachari, K.; Rendell, A.; Burant, J. C.; Iyengar, S. S.; Tomasi, J.; Cossi, M.; Rega, N.; Millam, J. M.; Klene, M.; Knox, J. E.; Cross, J. B.; Bakken, V.; Adamo, C.; Jaramillo, J.; Gomperts, R.; Stratmann, R. E.; Yazyev, O.; Austin, A. J.; Cammi, R.; Pomelli, C.; Ochterski, J. W.; Martin, R. L.; Morokuma, K.; Zakrzewski, V. G.; Voth, G. A.; Salvador, P.; Dannenberg, J. J.; Dapprich, S.; Daniels, A. D.; Farkas, Ö.; Foresman, J. B.; Ortiz, J. V.; Cioslowski, J.; Fox, D. J. , Gaussian, Inc, Wallingford CT, 2009.
[24] L.A. Curtiss, P.C. Redfern, K. Raghavachari, J. Chem. Phys. 126 (2007) -.
[25] J. Aguilera-Iparraguirre, H.J. Curran, W. Klopper, J.M. Simmie, J. Phys. Chem. A 112 (2008) 7047-7054.
[26] H.-H. Carstensen, A.M. Dean, O. Deutschmann, Proc. Combust. Inst. 31 (2007) 149-157.
[27] A.G. Baboul, L.A. Curtiss, P.C. Redfern, K. Raghavachari, J. Chem. Phys. 110 (1999) 7650-7657.
[28] C. Eckart, Phys. Rev. 35 (1930) 1303-1309.
[29] E. Wigner, Phys. Rev. 40 (1932) 749-759.
[30] S. Canneaux, F. Bohr, E. Henon, J. Comput. Chem. 35 (2014) 82-93.
[31] D.R. Glowacki, C.-H. Liang, C. Morley, M.J. Pilling, S.H. Robertson, J. Phys. Chem. A 116 (2012) 9545-9560.
[32] J.T. Bartis,B. Widom, J. Chem. Phys. 60 (1974) 3474-3482.
[33] S.J. Klippenstein, RRKM theory and its implementation, in Comprehensive Chemical Kinetics, N.J.B. Green, Editor. 2003, Elsevier. p. 55-103.
[34] J.W. Davies, N.J.B. Green, M.J. Pilling, Chem. Phys. Lett. 126 (1986) 373-379.
[35] RC Handbook of Chemistry and Physics: a Ready-Reference Book of Chemical and Physical Data, ed. D.R. Lide. 2008, London: CRC, Boca Raton.
[36] R.Y. Luo, Handbook of Bond Dissociation Energies in Organic Compounds. 1999, Florida, Boca Raton: CRC Press.

[37] Z. Wang, Y. Li, F. Zhang, L. Zhang, W. Yuan, Y. Wang, F. Qi, Proceedings of the Combustion Institute 34 (2013) 1785-1793.
[38] J.M. Simmie, J. Phys. Chem. A 116 (2012) 4528-4538.
[39] D.L. Baulch, C.T. Bowman, C.J. Cobos, R.A. Cox, T. Just, J.A. Kerr, M.J. Pilling, D. Stocker, J. Troe, W. Tsang, R.W. Walker, J. Warnatz, J. Phys. Chem. Ref. Data 34 (2005) 757-1397.
[40] W. Tsang, J. Phys. Chem. Ref. Data 17 (1988) 887-951.
[41] J.P. Orme, H.J. Curran, J.M. Simmie, J. Phys. Chem. A 110 (2005) 114-131.
[42] R.R. Baldwin, R.W. Walker, Symp. Int. Combust. Proc. 17 (1979) 525-533.
[43] M. Altarawneh, B.Z. Dlugogorski, E.M. Kennedy, J.C. Mackie, Proc. Combust. Inst. 34 (2013) 315-323.
[44] G. da Silva ,J.W. Bozzelli, Proc. Combust. Inst. 32 (2009) 287-294.
[45] D. Truhlar, G,B. Garrett, C, Ann. Rev. Phys. Chem. 35 (1984) 159-89.
[46] M. Altarawneh, B.Z. Dlugogorski, E.M. Kennedy, J.C. Mackie, J. Phys. Chem. A 112 (2008) 3680-3692.
[47] M. Altarawneh,B.Z. Dlugogorski, J. Phys. Chem. A 118 (2014) 9338-9346.
[48] Z. Hong, D.F. Davidson, K.-Y. Lam, R.K. Hanson, Combust. Flame 159 (2012) 3007-3013.
[49] Z. Hong, R.D. Cook, D.F. Davidson, R.K. Hanson, J. Phys. Chem. A 114 (2010) 5718-5727.
[50] H.Y. Afeefy, J.F. Liebman, S.E. Stein, P.J. Linstrom, W.G. Mallard, NIST Chemistry WebBook, NIST Standard Reference Database Number 69. 2005.

Table 1

$\Delta_f H°_{298}$ for reference species [50] used in the isodesmic reactions. All values are in kcal mol^{-1}.

Compound	$\Delta_f H°_{298}$	Compound	$\Delta_f H°_{298}$
$C_6H_5CH_2CH_3$	7.10 ± 0.20	$C_6H_5CH_3$	12.0 ± 0.26
$C_6H_5CH_2CH_2CH_3$	1.90 ± 0.20	$CH_3CH_2CH_3$	-25.0 ± 0.20
$C_6H_5CHCH_3$	40.4 ± 0.5	CH_3CH_3	-20.0 ± 0.10
$C_6H_5CH_2CH_2$	55.9 ± 0.5	$CH_3CH_2CH_2$	23.9 ± 0.50
CH_3CHCH_3	21.0 ± 0.50	CH_3CH_2	28.4 ± 0.20
$CH_3CH_2CH_2CH_3$	-30.0 ± 0.16	$CH_3CH_2CHCH_3$	16.0 ± 0.50

Table 2

$\Delta_f H°_{298}$ computed for propylbenzene and its three derived radicals. All values are in kcal mol^{-1}.

		Calculated $\Delta_f H°_{298}$				Calculated uncertainty		Literature $\Delta_f H°_{298}$	Refs
		CBS-QB3	G3MP2B3	x_j	$\bar{x}$	u_j	$\bar{u}$		
$C_6H_5CH_2CH_2CH_3$	IR1a	1.4	1.5	1.4	2.6	0.3	0.2	1.9 ± 0.2	[50]
	IR1b	1.1	1.1	1.1		0.3			
$C_6H_5CHCH_2CH_2$	IR2a	39.1	41.2	40.2	39.6	1.7	1.2	35.2	[9]
	IR2b	37.8	40.3	39.0		1.8			
$C_6H_5CH_2CHCH_3$	IR3a	48.3	48.6	48.4	48.6	0.4	0.4	48.9	[9]
	IR3b	49.2	49.6	49.4		0.8			
$C_6H_4CH_2CH_2CH_2$	IR4a	51.1	51.2	51.1	51.0	0.7	0.5	50.0	[9]
	IR4b	50.9	51.0	50.9		0.7			

Table 3

Kinetic parameters for abstraction of an H atom from the propyl side chain in *n*-propylbenzene, by HO_2. Parameters are fitted in the temperature range of 300-1500 K. Reaction ($\Delta_r H°_{298}$) and activation enthalpies ($\Delta H^{\#}$) are in kcal and kcal mol^{-1}, respectively. Reaction degeneracy is incorporated in fitted reaction rate constants.

Products	$\Delta_r H°_{298}$	$\Delta H^{\#}$		A (cm^3 $molecule^{-1}$ s^{-1})	E_a (cal mol^{-1})
$C_6H_5CHCH_2CH_3$ (R1) + H_2O_2	1.4	13.0	Eckart	8.00×10^{-13}	12 100
			Wigner	8.93×10^{-12}	12 000
$C_6H_5CH_2CHCH_3$ (R2) + H_2O_2	11.8	13.2	Eckart	7.50×10^{-13}	13 000
			Wigner	5.54×10^{-13}	12 100
$C_6H_5CH_2CH_2CH_2$ (R3) + H_2O_2	14.5	17.5	Eckart	1.19×10^{-12}	16 700
			Wigner	2.31×10^{-12}	15 900

Table 4

Kinetic parameters for abstraction of H atom by HO_2 radicals from different compounds. Reaction rate constants are fitted in the temperature range of 400-1600 K. Reaction enthalpies ($\Delta_r H°_{298}$), activation enthalpies ($\Delta H^{\#}$) and energies of activations (E_a) are in kcal, for $\Delta_r H°_{298}$, and kcal mol^{-1}, for $\Delta H^{\#}$ and E_a. Values of A factors and $k(T)$ are in cm^3 $molecule^{-1}$ s^{-1} per one H site. [a]Ref [25]

		$\Delta_r H°_{298}$	$\Delta H^{\#}$	A	E_a	$k(T)$	
						600 K	800 K
Primary	$CH_3CH_2CH_3$	14.2	17.9	8.57×10^{-13}	16.9	6.00×10^{-19}	2.02×10^{-17}
						$[3.22 \times 10^{-19}]^a$	$[3.48 \times 10^{-17}]^a$
	$CH_3CH_2CH_2CH_3$	14.5	17.6	8.13×10^{-13}	16.6	8.09×10^{-19}	2.37×10^{-17}
						$[4.90 \times 10^{-19}]^a$	$[5.00 \times 10^{-17}]^a$
	$CH_3CH_2CH_2CH_2CH_3$	14.2	17.5	1.64×10^{-13}	16.5	1.69×10^{-19}	4.95×10^{-18}
	$C_6H_5CH_2CH_3$	14.6	17.9	4.23×10^{-13}	16.4	3.21×10^{-19}	1.09×10^{-17}
	$C_6H_5CH_2CH_2CH_3$	14.5	17.5	4.00×10^{-13}	16.7	9.85×10^{-19}	2.76×10^{-17}
Secondary	$CH_3CH_2CH_3$	11.2	14.2	9.50×10^{-13}	13.1	1.60×10^{-17}	2.50×10^{-16}
						$[1.15 \times 10^{-17}]^a$	$[9.32 \times 10^{-17}]^a$
	$CH_3CH_2CH_2CH_3$	11.4	13.7	2.16×10^{-13}	12.7	6.67×10^{-18}	8.84×10^{-17}
						$[6.00 \times 10^{-18}]^a$	$[2.72 \times 10^{-16}]^a$
	$CH_3CH_2CH_2CH_2CH_3$	11.4	13.5	2.81×10^{-13}	12.4	8.56×10^{-18}	1.11×10^{-16}
	$C_6H_5CH_2CH_2CH_3$	11.8	13.2	2.00×10^{-13}	12.1	7.82×10^{-18}	9.90×10^{-17}
Benzylic	$C_6H_5CH_3$	2.9	12.5	2.11×10^{-14}	12.2	7.58×10^{-19}	9.79×10^{-18}
	$C_6H_5CH_2CH_3$	0.8	11.2	1.02×10^{-13}	12.3	3.37×10^{-18}	4.44×10^{-17}
	$C_6H_5CH_2CH_2CH_3$	1.4	13.0	2.67×10^{-13}	12.1	1.04×10^{-17}	1.32×10^{-16}

Table 5

Kinetic parameters at the high-pressure limit for unimolecular decomposition of the three HO_2-phenylpropyl adducts (M1, M2, M3), fitted in the temperature range of 300-1500 K.

Reaction	A (s^{-1})	n	E_a (cal mol^{-1})
M1 → R1 + HO_2	8.72×10^{11}	1.08	58 500
M1 → M5 + OH	1.42×10^{10}	1.81	41 700
M1 → M4 + H_2O (TS1)	6.71×10^{13}	0.00	41 100
M1 → M4 + H_2O(TS2)	9.97×10^{11}	0.66	42 400
M1 → M7	1.41×10^{14}	-0.35	58 800
M1 → M8 + H_2O	2.48×10^{13}	0.00	66 800
M1 → M6 + OH	7.26×10^{13}	0.00	42 500
M5 → M9+ C_2H_5	1.20×10^{11}	0.79	3 900
M2 → R2 + HO_2	4.78×10^{11}	1.45	69 000
M2 → M11 + OH	2.46×10^{15}	0.00	44 200
M2 → M10 + H_2O (TS8)	3.36×10^{13}	0.00	39 900
M2 → M10 + H_2O (TS9)	5.26×10^{12}	0.00	50 500
M2 → M12 + OH	7.62×10^{14}	0.00	41 000
M11 → M14 + $CH_3C(H)O$	2.94×10^{12}	0.00	6 000
M3 → R3 + HO_2	5.18×10^{10}	1.62	68 100
M3 → M17 + OH	2.95×10^{10}	1.61	42 800
M3 → M15 + H_2O (TS13)	1.80×10^{13}	0.00	38 600
M3 → M15 + H_2O (TS14)	6.97×10^{13}	0.00	47 100
M3 → M16 + OH	3.78×10^{13}	0.00	53 700
M17 → M18 + CH_2O	1.14×10^{14}	0.00	13 300

Table 6

Kinetic parameters for HO_2 addition (i.e. addition by termination) to the three phenylpropyl radicals (R1, R2 R3), fitted in the temperature range of 300-1500 K.

Reaction	*A* (cm^3 $molecule^{-1}$ s^{-1})	*E*a (cal mol^{-1})
R1 + HO_2 → M1	7.94×10^{-14}	- 2 200
R2 + HO_2 → M2	8.57×10^{-13}	- 2 500
R3 + HO_2 → M3	1.54×10^{-12}	- 2 800

Table 7

Phenomenological rate coefficients at 1.0 atm. Values are in s^{-1} or cm^3 molecule^{-1} s^{-1}. .

	T (K)		
Reaction	600	800	1000
R1 + HO_2 → M1	9.33×10^4	4.86×10^4	7.29×10^3
M1 → M4	8.44×10^{-3}	43.71	1.70×10^3
M1 → M5 + OH	1.75×10^{-2}	89.82	3.47×10^3
M1 → M6 + OH	3.69×10^{-4}	4.39	2.20×10^2
R2 + HO_2 → M2	1.15×10^5	7.86×10^4	3.07×10^4
M2 → M10 + H_2O	7.98×10^{-4}	10.63	2.01×10^3
M2 → M11 + OH	1.78×10^{-2}	150.00	2.22×10^4
R3 + HO_2 → M3	1.05×10^5	2.86×10^4	1.71×10^3
M3 → M15 + H_2O	0.17	5.13×10^2	2.15×10^4
M3 → M17 + OH	0.56	3.74×10^3	2.00×10^5

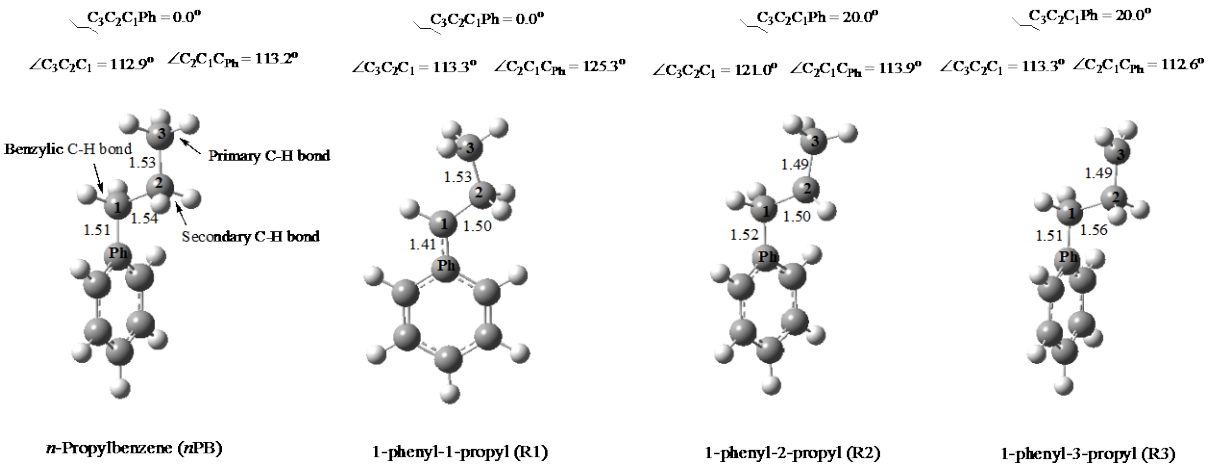

Fig. 1. Optimised geometries of *n*-propylbenzene and its three derived phenylpropyl radicals.

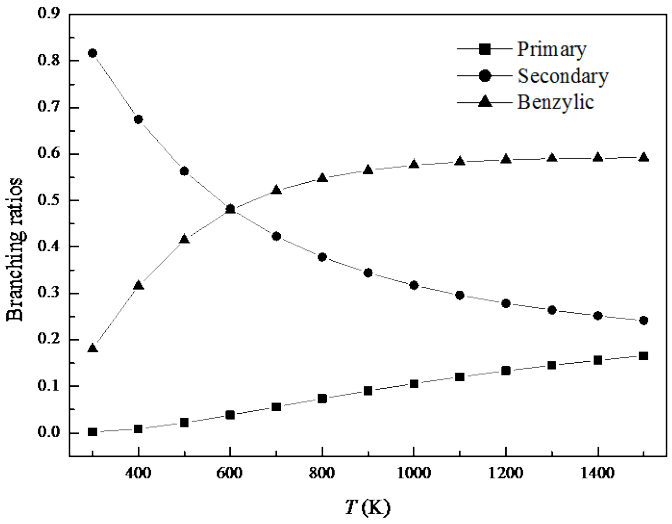

Fig. 2. Branching ratios for H abstraction by HO_2 radicals from primary, secondary and benzylic sites in *n*-propylbenzene.

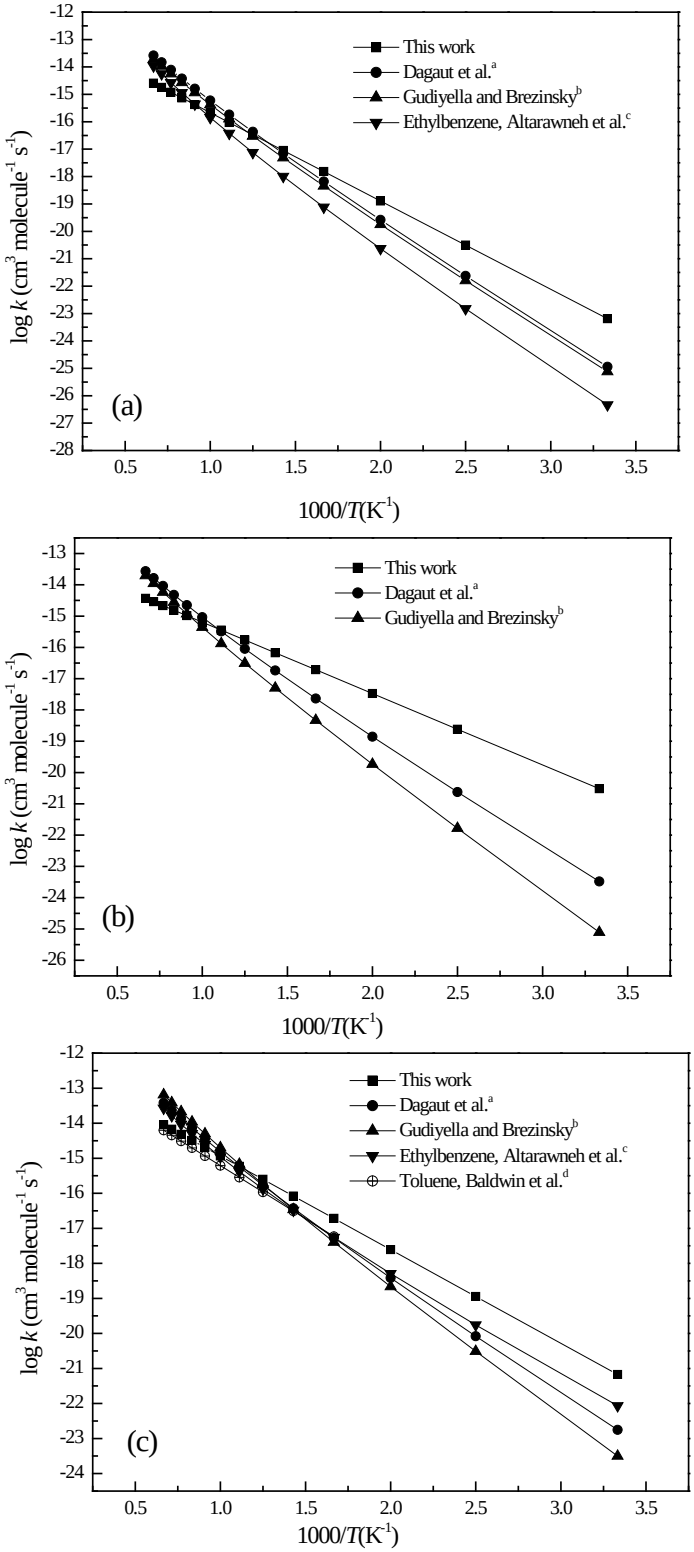

Fig. 3. Comparisons between calculated and literature values for H abstraction by HO_2 radicals from primary (a), secondary (b) and benzylic sites (c) in *n*-propylbenzene. [a]Ref [9], [b]Ref [11], [c]Ref [22], [d]Ref [39]

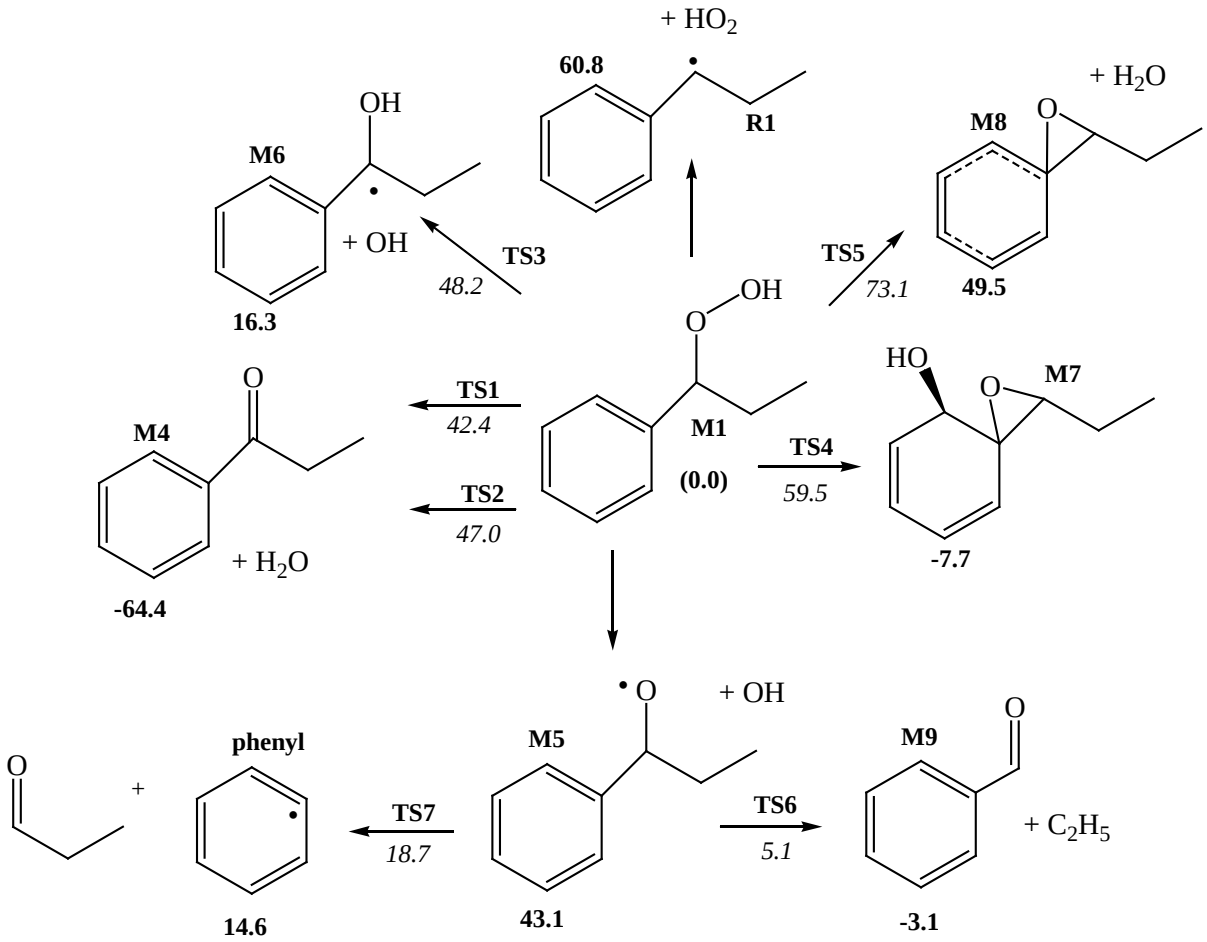

Fig. 4. Unimolecular decomposition of HO_2-1-phenyl-1-propyl adduct (M1). Values in bold and italic denote reaction (in kcal) and activation enthalpies (in kcal mol^{-1}), respectively, calculated at 298.15 K.

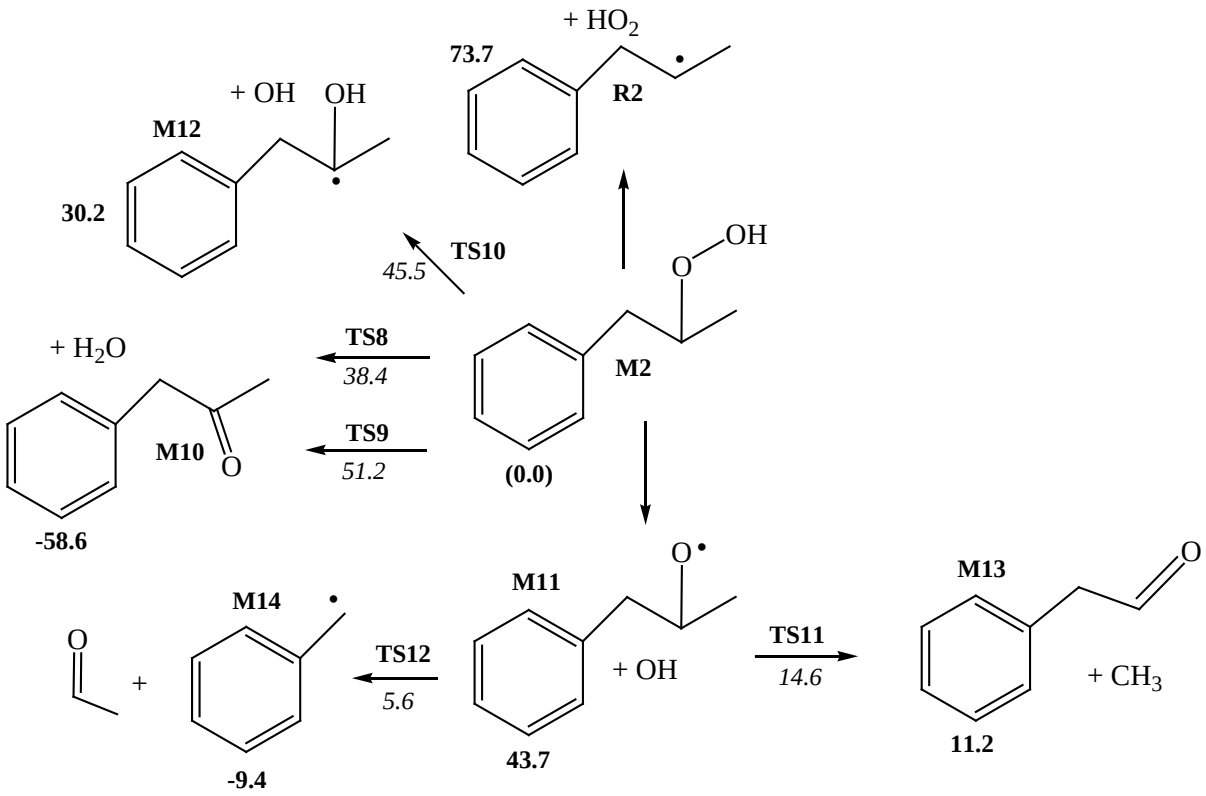

Fig. 5. Unimolecular decomposition of HO_2-1-phenyl-2-propyl adduct (M2). Values in bold and italic denote reaction (in kcal) and activation enthalpies (in kcal mol^{-1}), respectively, calculated at 298.15 K.

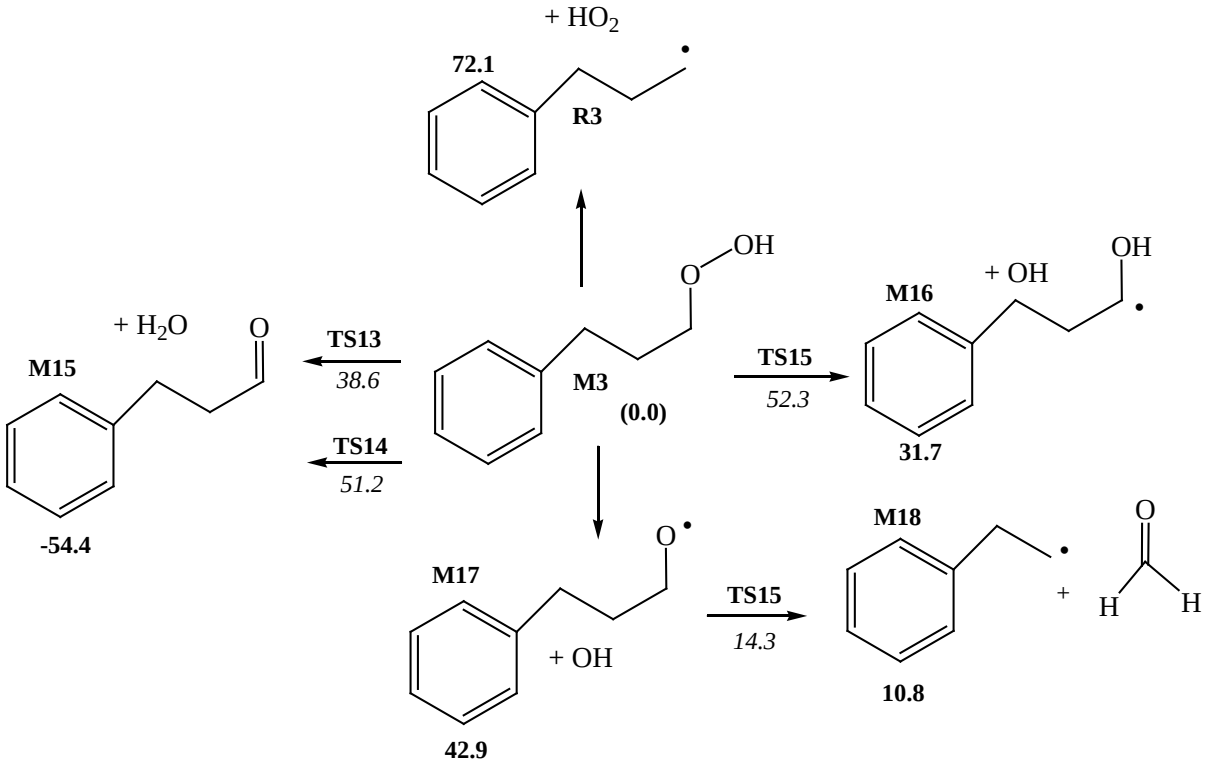

Fig. 6. Unimolecular decomposition of HO_2-1-phenyl-3-propyl adduct (M3). Values in bold and italic denote reaction (in kcal) and activation enthalpies (in kcal mol^{-1}), respectively, calculated at 298.15 K.

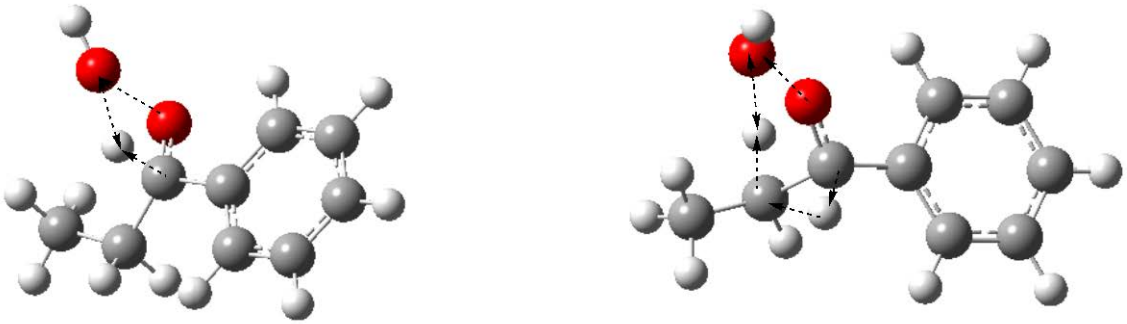

TS1 TS2

Fig. 7. Atomic movements in transition structures, TS1 and TS2.

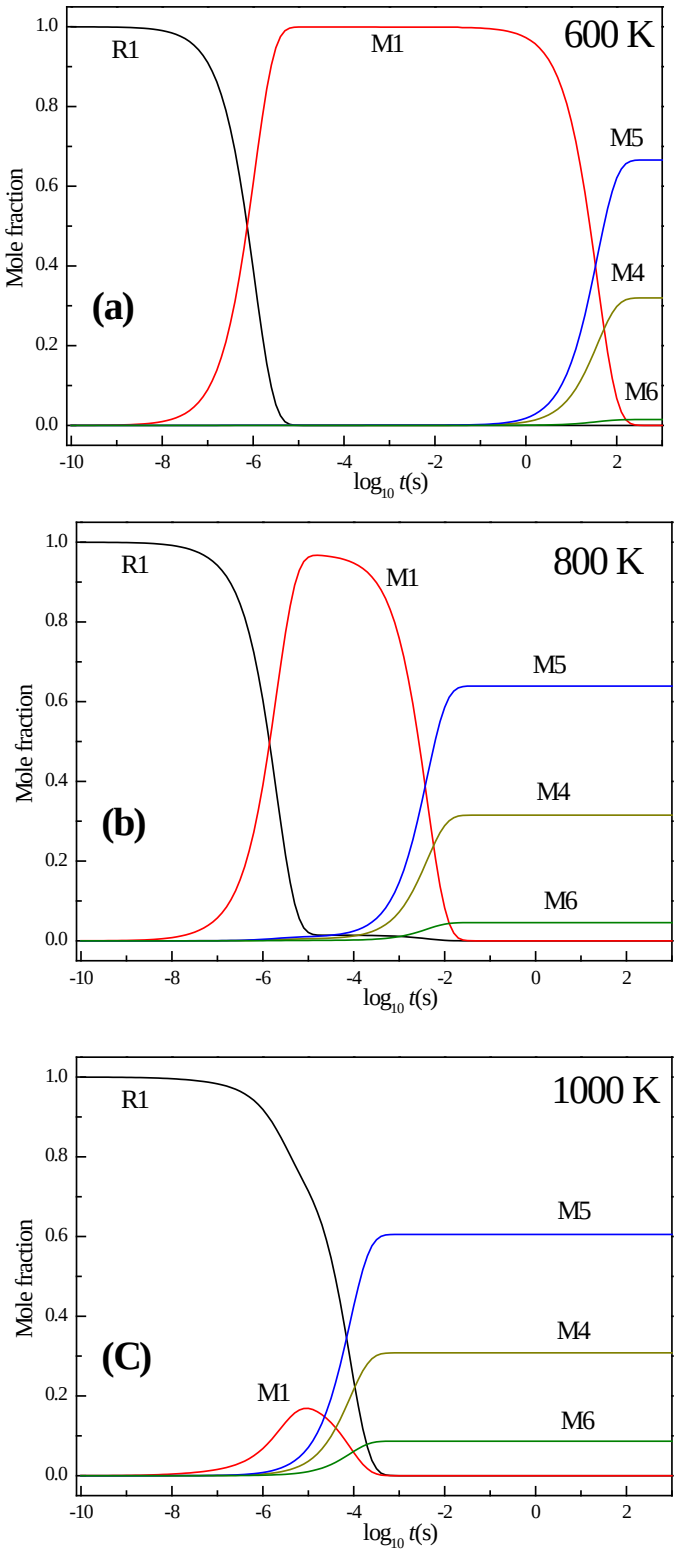

Fig. 8. Species time profiles for the R1 + HO_2 system calculated at 1.0 atm.

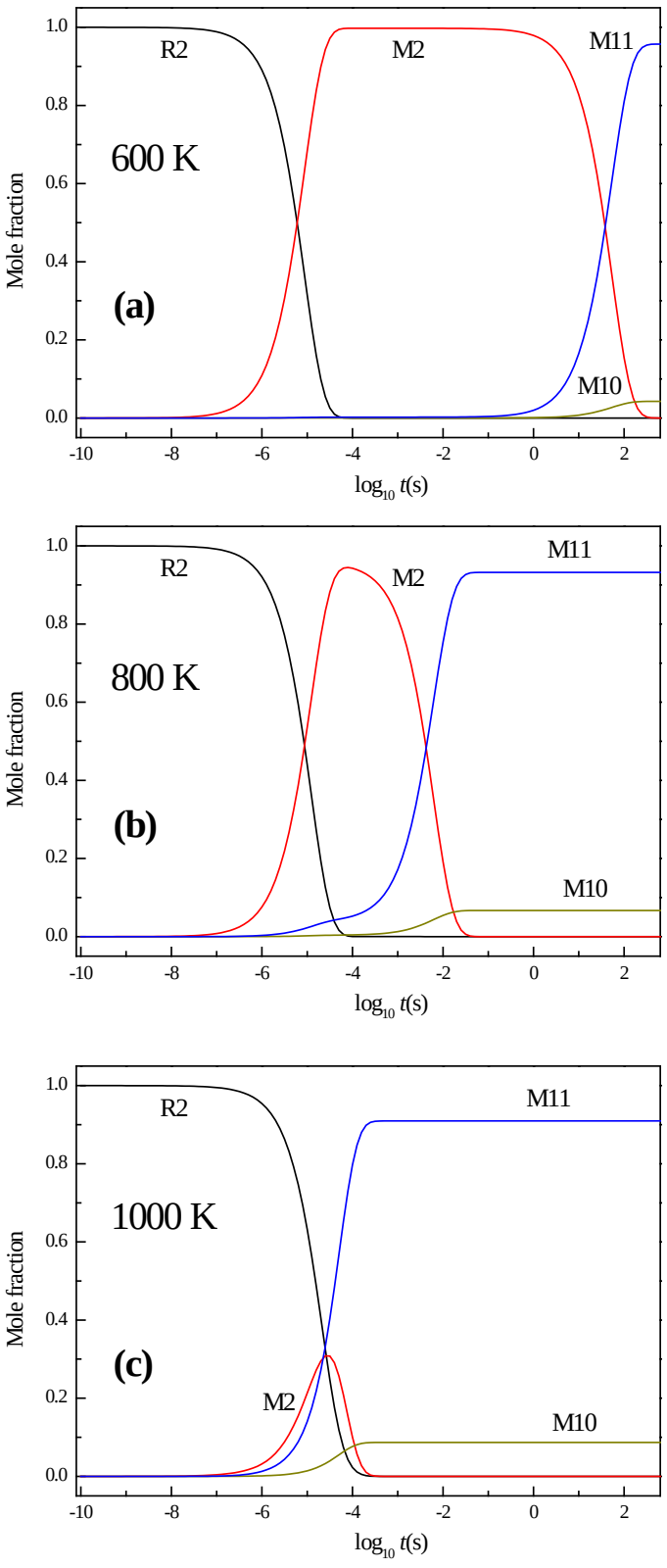

Fig. 9. Species time profiles for the R2 + HO_2 system calculated at 1.0 atm.

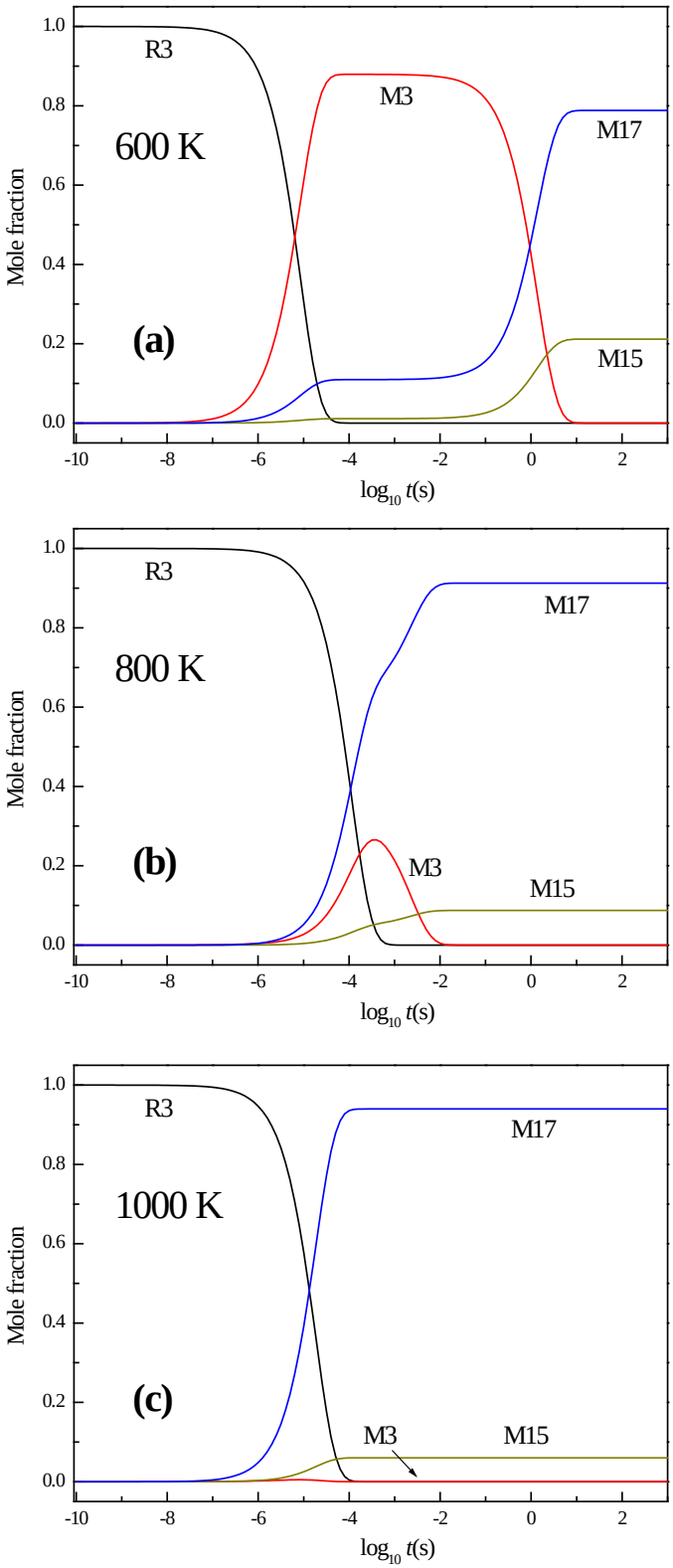

Fig. 10. Species time profiles for the R3 + HO_2 system calculated at 1.0 atm.